Proceedings of the Twenty-third (2013) International Offshore and Polar Engineering **www.isope.org**
Anchorage, Alaska, USA, June 30–July 5, 2013

ISBN 978-1-880653-99–9 (Set); ISSN 1098-6189 (Set)

Analysis of Floating Offshore Wind Turbine Hydrodynamics Using coupled CFD and Multibody Methods

Friedemann Beyer, Matthias Arnold and Po Wen Cheng
Stuttgart Chair of Wind Energy (SWE), University of Stuttgart,
Stuttgart, Germany

ABSTRACT

The focus of this study is the application of a higher order hydrodynamic modeling technique for the analysis of Floating Offshore Wind Turbine dynamics. This approach is based on a coupling between Multibody and Computational Fluid Dynamics methods. Results of the translational and rotational platform displacement are presented for a basic free-decay simulation in surge direction in still water. A comparison to linear hydrodynamics is presented. Additional, pressure mapping is demonstrated.

KEY WORDS: Floating offshore wind turbine (FOWT) dynamics; multibody (MBS); computational fluid dynamics (CFD); pressure mapping; hydrodynamics

INTRODUCTION

From an academic point of view research about Floating Offshore Wind Turbines (FOWT) is very interesting due to increased complexity in modeling and simulation. Additional Degrees-of-Freedom (DOF) of the floating platform introduce transient aerodynamic and hydrodynamic effects onshore or fixed-bottom offshore wind turbines are not exposed to. The industry has realized the potential of FOWTs and first prototypes have been deployed starting in 2007. Besides multiple conceptual studies like the OC3-Hywind spar-buoy (Jonkman, 2010) or the OC4-DeepCwind semisubmersible (Robertson et al., 2012) further full scale prototypes are planned to be installed in 2013 and ongoing within the EU project HiPRWind (2013) and FLOATGEN (Recharge, 2013). Immense offshore wind resources over deep water (Musial and Butterfield, 2004) motivate the development of new floating technologies.
FOWTs have several advantages from a power generation perspective like stronger, more consistent and more predictable winds compared to onshore. They can be placed flexible to avoid shipping lanes and other critical zones and to minimize visual impact near the coastline. On the other hand researchers and designers have to handle a more complex dynamic behavior.
During a design process cost effective solutions of FOWTs are desired. Sophisticated design tools that are able to model and simulate the dynamics of the integrated floating system are necessary. The diversity of load case scenarios that can be simulated is of importance but also the fidelity that can be achieved.

METHODOLOGY

This paper presents an approach for modeling and simulation of an integrated wind turbine-floater system based on a coupling of Multibody and Computational Fluid Dynamics methods.

Multibody Approach

The structure of the wind turbine and floating platform is modeled by means of the Multibody System (MBS) software SIMPACK. This commercial, fully coupled and validated aero-servo-hydro-elastic wind turbine simulation tool has the capabilities of incorporating modally reduced flexible Finite Element Methods (FEM) bodies and applying complex aerodynamic force elements based on Blade Element Momentum (BEM), Free Vortex and Computational Fluid Dynamics (CFD) methods. The bodies of the wind turbine model are connected by joints of various type. Hydrodynamic forces are calculated via a coupling to NREL's software package HydroDyn (Jonkman and Jonkman, 2010) which considers the linear hydrostatic restoring, added mass and damping contributions from linear wave radiation with inclusion of free surface memory effects, incident wave excitation from linear diffraction and nonlinear viscous drag (Cordle and Jonkman, 2011). A quasi-static mooring line model is used to apply restoring forces. This MBS approach enables great flexibility in terms of modeling and fidelity of an integrated wind turbine-floater system.
Linear Airy wave theory is applied to calculate incident-wave kinematics in HydroDyn due to the assumption of hydrodynamic linearity. Thus, steep or breaking waves in either deep or shallow water and the resulting slap and slam loading cannot be modeled (Matha et al., 2011) and require higher-order wave kinematics theories.

Computational Fluid Dynamics Approach

Methods of higher fidelity are used in this research to overcome the presented limitations. Flow-induced hydrodynamic loads are simulated with the commercially available CFD code ANSYS CFX. It uses the Finite-Volume Method to solve the Reynolds-Averaged Navier-Stokes

(RANS) equations on structured and unstructured grids and is coupled to the MBS tool. The interface between the liquid (water) and gas (air) represents a free surface that is modeled via the Volume of Fluid (VOF) approach. It computes the shape and location of the free surface on the basis of a fractional volume function (Ansys, 2013). The coupling between CFX and SIMPACK has been developed by Arnold et al. (2013) for the simulation of fluid-structure-interaction on tidal current turbines. Arnold demonstrates the validity of the coupling based on a code-to-code comparison of the simulation of a bisymmetric rotor blade of a tidal current turbine. Thus, the scope of this research does not primarily focus on the validation of the developed numerical code.
Besides the incorporation of higher-order effects the proposed approach inherently provides a detailed pressure and loads distribution on the hull of the floating platform. Computation of the pressure field using common linear or non-linear hydrodynamics modeling techniques is complicated. Especially complex floater geometries for example with several columns and pontoons, can be analyzed with the presented technique to a higher level of detail and thus benefit the design process.

Motivation and Structure of the Coupling

Several aspects motivate the application of the coupling between CFX and SIMPACK. First of all, CFX is only able to implement rigid bodies in a standalone simulation. Applying a Fluid-Structure-Interaction (FSI) using FEM and CFD for complex structures requires unreasonable high computational resources. However, the dynamics of modally reduced flexible FEM bodies of the floating platform should be investigated in future analyses based on this research. The flexible bodies can be implemented within the MBS simulation environment. Secondly, the complexity of the rigid body in CFX is limited and only simple elements using spring-damper properties are possible. Thirdly and most important, an integrated aero-servo-hydro-elastic analysis of a FOWT cannot be performed in CFX standalone. The coupling to the MBS tool, however, enables the consideration of the mooring system, aerodynamic forces on the rotor and tower, the effect of the control system etc.
The coupling is controlled by means of a moderator script that on the one hand directs CFX to send loads/receive motion information to/from SIMPACK and on the other hand commands SIMPACK to send motion/receive loads information to/from CFX. A fully implicit iteration scheme is incorporated within the coupling for transient simulations.
Within SIMPACK, a user force element written in Fortran is implemented. This interface is named CFX2SPCK and used to read and transform loads and to measure and send deformations during a coupled simulation.

RESULTS AND DISCUSSION

Results of a coupled MBS and CFD simulation are obtained for a free-decay test of a simple floating platform in still water. Restoring forces are included by means of a quasi-static mooring system. A comparison to MBS standalone interfaced with HydroDyn is presented.

Simulation Parameters

The properties of the floating system are given in this section, as well as the load case and solver settings.

Floating System Properties

The properties of the wind turbine are based on the standardized "NREL offshore 5-MW baseline wind turbine" (Jonkman et al., 2009). A summary of the specifications is shown in Tab. 1.

Tab.1: Properties of the NREL 5-MW baseline wind turbine

Property	Value
Rating	5 MW
Rotor orientation, configuration	Upwind, 3 blades
Control	Variable speed, collective pitch
Drivetrain	High speed, multiple-stage gearbox
Rotor, hub diameter	126 m, 3 m
Hub height	90 m
Cut-in, rated, cut-out wind speed	3 m/s, 11.4 m/s, 25 m/s
Cut-in, rated rotor speed	6.9 rpm, 12.1 rpm
Rated tip speed	80 m/s
Overhang, shaft tilt, precone	5 m, 5°, 2.5°
Rotor mass	110 000 kg
Nacelle mass	240 000 kg
Tower mass (OC3 Phase IV)*	249 718 kg
Coordinate location of overall CM	(-0.2 m, 0 m, 64.0 m)

*Tower mass (baseline): 347 500 kg

The wind turbine is mounted to the conceptual floating platform OC3-Hywind spar-buoy which is described in Jonkman (2010) for Phase IV of the IEA Annex 23 Offshore Code Comparison Collaboration (OC3) project. A summary of the specifications is given in Tab. 2. An illustration of the NREL 5-MW wind turbine on the OC3-Hywind spar-buoy is presented in Fig. 1.

Tab. 2: Properties of the OC3-Hywind spar-buoy

Property	Value
Diameter	6.5 m to 9.4 m
Draft	120 m
Water displacement	8029 m^3
Mass, including ballast	7 466 330 kg
CM location below SWL	89.9155 m
Roll inertia about CM	4 229 230 000 kgm^2
Pitch inertial about CM	4 229 230 000 kgm^2
Yaw inertia about CM	164 230 000 kgm^2

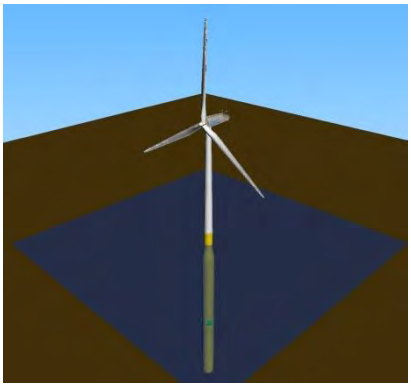

Fig. 1: Illustration of the OC3-Hywind floating system

Load Case Definition

A simple free-decay test in platform surge that is derived from load case specification 1.4 in the OC3 project Phase IV (J. Jonkman and Musial 2010) has been chosen. A summary of the specifications is given in Tab. 3. All translational (surge, sway) and rotational (roll, pitch, yaw) platform DOFs are enabled except for the heave motion due

to numerical instabilities during the first iterations of the coupled simulation.

Tab. 3: Summary of load case parameters

Initial Condition	Enabled DOFs	Wind Condition	Wave Condition
Platform surge = +21 m	Platform: Surge, sway, roll, pitch, yaw	No wind	Still water

Mesh Properties

The dimensions of the fluid domain which is shown in Fig. 2 are 650 m in width and depth and 370 m in height (320 m below Still Water Level (SWL), 50 m above SWL). The mesh is discretized into a structured grid consisting of 621 000 hexahedra elements. The boundary conditions are summarized in Tab. 4.

Tab. 4: Summary of applied boundary conditions

Boundary Condition	Specifications
FARFIELD	- Wall - Free-slip condition (no wall friction effects) - Stationary mesh
PLATFORM	- Wall - No-slip condition (wall friction effects) - Specified mesh displacement
SEABED	- Wall - Free-slip condition (no wall friction effects) - Mesh motion parallel to the boundary
TOP	- Opening - Mesh motion parallel to the boundary - Constant atmospheric pressure - Constant volume fractions (100% air and 0% water)

The hydrostatic pressure distribution is initialized in the domain and the volume fractions are set constant with respect to the z-axis (100% water for $z \leq 0$ m). A subdomain for the NEARFIELD of the floating platform is set up with the dimensions of 30 m x 30 m x 170 m and moved with a specified mesh displacement (see Fig. 3). It is computed locally during the coupled simulation. The moving mesh methodology is described in more detail by Arnold et al. (2013).

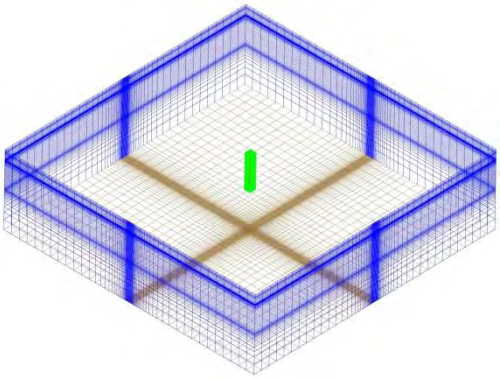

Fig. 2: Illustration of the mesh and boundary conditions of the fluid domain (blue: FARFIELD, brown: SEABED, green: Subdomain NEARFIELD with PLATFORM inside, TOP invisible)

The mesh is refined near the water surface to be able to simulate waves radiated by the platform. Grid cells are also placed with a higher density close to the surface of the floater (see Fig. 3) to resolve the boundary layer and obtain sufficient viscous damping.

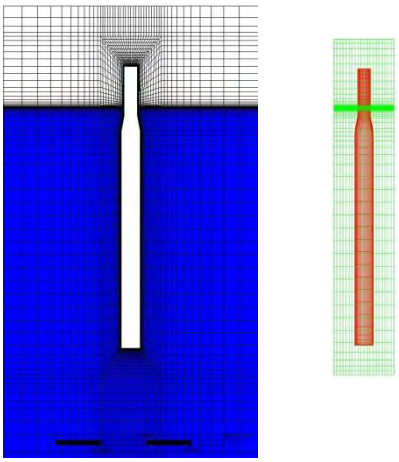

Fig. 3: Illustration of the mesh at the NEARFIELD subdomain that includes the floating platform (Left: blue: volume fraction of 100% water, white: volume fraction of 100% air except for the interior of the platform; Right: green: Subdomain NEARFIELD, red: PLATFORM)

Poles of the mesh stiffness had to be introduced to reduce the mesh displacement gradient to zero. This was necessary due to high relative motions of the floater resulting in a deformed and corrupted mesh near critical points that caused the solver to abort. The quality of the mesh could be increased with a hyperbolic function of the mesh stiffness $\zeta(x,y,z)$ that is described by Schildhauer (2011). For a number of n poles at three-dimensional positions (x_{pi}, y_{pi}, z_{pi}) the resulting mathematical statement is given in Eq. 1:

$$\zeta(x,y,z) = \mathrm{C} \cdot \left[\sum_{i=1}^{n} \left(\frac{1}{\sqrt{(x-x_{pi})^2 + (y-y_{pi})^2 + (z-z_{pi})^2}} \right)^c \right] \quad (1)$$

The dimensional constant C is used for scaling of the function and the exponent c determines the strength of the pole. The higher c the more the effect of the pole is geometrically pushed away from (x_{pi}, y_{pi}, z_{pi}). The critical points were identified at the upper and lower corner vertices of the NEARFIELD subdomain and the coordinates are summarized in Tab. 5.

Tab. 5: Coordinates of the poles of the mesh stiffness

x [m]	y [m]	z [m]
+15	+15	+35
-15	+15	+35
-15	-15	+35
+15	-15	+35

x [m]	y [m]	z [m]
+15	+15	-135
-15	+15	-135
-15	-15	-135
+15	-15	-135

The hyperbolic function of the mesh stiffness is illustrated on the left of Fig. 4 in dependence of the coordinates x and y for clarification of Eq. 1. Instead of the coordinates given in Tab. 5 the poles are at positions [1 1], [-1 1], [-1 -1] and [1 -1]. On the right of Fig. 4, the strength of the mesh stiffness is represented by colored slices in the three-dimensional x-y-z domain. It can be seen as an illustration of the distribution of the mesh stiffness along the cuboid-shaped NEARFIELD subdomain except that the poles are at coordinates z = 1 m and z = *-1 m.*

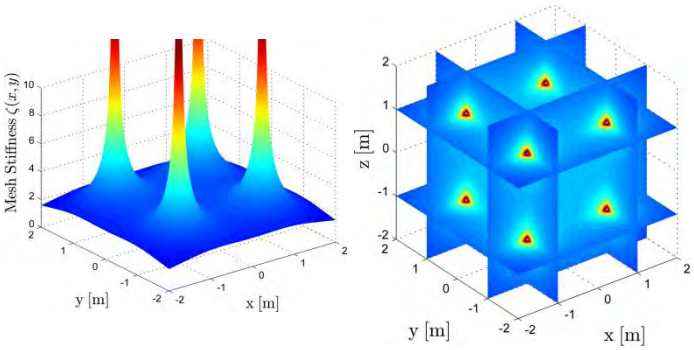

Fig. 4: Left: two-dimensional illustration of the mesh stiffness $\zeta(x,y)$, Right: three-dimensional illustration of the mesh stiffness $\zeta(x,y,z)$, Both: $C = 1\ m^2/s$, $c = 1$

Model and Solver Settings

The main model and solver parameters are summarized in Tab. 6.

Tab. 6: CFX and SIMPACK Solver Settings

Parameter	Setting
CFX: Physical Model	
Multiphase model	Homogen
Turbulence model	SST
CFX: Fluid Properties	
Density air	$\rho_{air} = 1.185\ kg/m^3$
Dynamic viscosity air	$\mu_{air} = 1.831 \cdot 10^{-5}\ kg/ms$
Density water	$\rho_{water} = 1025\ kg/m^3$
Dynamic viscosity water	$\mu_{water} = 8.899 \cdot 10^{-4}\ kg/ms$
CFX: Initialization	
Velocity	$u = v = w = 0\ m/s$
Pressure	Hydrostatic pressure distribution
Volume fraction	Constant ($z \leq 0$ m: 100% water)
Gravity	$g = 9.81\ m/s^2$
CFX: Solver	
Analysis Type	Transient
Time Step	$dt = 1.0$ s
Transient Scheme	1st order Backward Euler
Turbulence Numerics	1st order
Convergence Criteria (RMS)	$1 \cdot 10^{-4}$
SIMPACK: Solver	
Integration Method	SODASRT 2
Platform	Rigid Body

Load Case 1.4: Free-Decay (Surge)

The simulation length is $t_{simu} = 300$ s. The platform is moored by three catenary lines with an angle of 120° between adjacent lines in order to include restoring forces. The fairleads are attached to the platform 70 m below the SWL. Additional properties are described by Jonkman (2010). The nonlinear restoring loads from the mooring system are calculated using a quasi-static approach implemented within HydroDyn. A static equilibrium is assumed to calculate the tensions within each mooring line for a given fairlead position. Thus, damping and inertia of the mooring system are ignored (Jonkman, 2007) and transient dynamic effects are neglected.

To avoid any conflicts in MBS between the new user force element CFX2SPCK and other force and control elements (e.g. pitch controller, aerodynamics), only the platform and mooring system are modeled for the coupled and standalone simulation in this research. However, the overall weight of the floating system needs to balance with the buoyancy. Thus, a rigid body (solid sphere of radius $R = 1$ m) with a mass equivalent to the weight of the rotor-nacelle assembly and the tower is mounted to the top of the platform using a 0-DOF joint. Using this modeling simplification the inertia of the floating system, however, is different compared to a fully integrated model of the wind turbine.

Platform Surge and Pitch Motion

Excitation of platform surge and pitch motion is predominant in this load case and results are shown in Fig. 5 and 6. Solid lines (black) refer to the coupled simulation (MBS+CFD), dashed lines (blue, green, red) to MBS standalone interfaced with HydroDyn (MBS+HydroDyn) and dash-dot lines (cyan) to NREL's wind turbine design tool FAST. The latter is used to simulate the fully integrated model of the OC3-Hywind spar-buoy according to the specifications.

The mesh at the boundary layer of the platform is resolved sufficiently to include viscous damping in CFD. The rigid body used for simple modeling of the rotor-nacelle assembly and the tower does not influence the surge motion if results of MBS+HydroDyn+AddDamping are compared to FAST. Applying linear hydrodynamics (MBS+HydroDyn) additional linear damping (AddDamping) is added to the linear radiation damping from potential flow theory and the nonlinear viscous-drag from Morison's equation to match with measurement data of the Hywind system (Jonkman, 2010). Results of platform surge almost converge for MBS+CFD and MBS+HydroDyn if the additional damping is reduced. The deviation can be decreased further by reduction of the empirical hydrodynamic viscous drag coefficient (PtfmCD) from 0.6 to 0.5 used for calculation of viscous drag from Morison's equation. Results of MBS+CFD and MBS+HydroDyn (reduced PtfmCD) show a good agreement in terms of amplitude and damping. However, the frequency of the damped oscillation in surge (approximately 0.008 Hz) is higher using coupled MBS and CFD. Thus, CFD predicts less added-mass contributions than linear hydrodynamics.

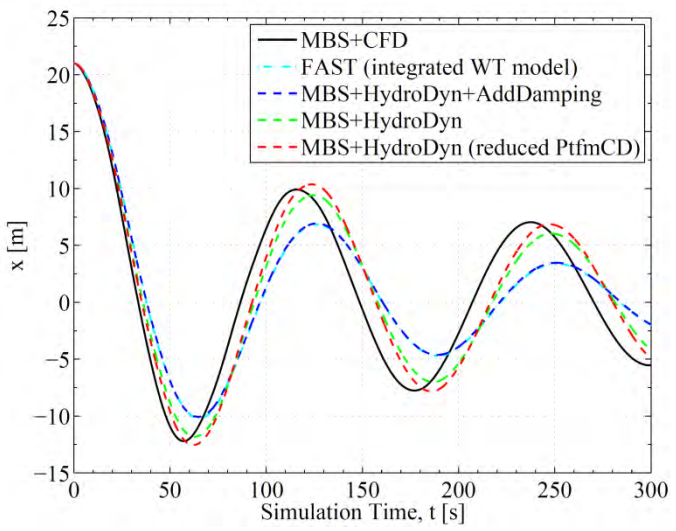

Fig. 5: Platform surge motion

The influence of friction between the fluid and the structure in the boundary layer is ignored in hydrodynamics based on potential flow theory. It may be introduced by the additional linear damping. A reason for differences between methods may be the application of the simplified wind turbine model that does not account for aerodynamic damping of the rotor-nacelle-assembly and tower. This effect in turn is included in the measurement data of the Hywind system and the resulting additional linear damping. However, the influence of aerodynamic drag is assumed to be small due to the low platform velocities during the free-decay.

Excitation of the platform pitch motion is small and significantly below β = 1°. A comparison to the fully integrated model applied in FAST demonstrates the impact of the inertia of the simplified floating system on the pitch DOF. Just like for the surge motion, the results of platform pitch of MBS and CFD on the one hand and MBS and linear hydrodynamics on the other hand converge if the additional linear damping and the viscous drag coefficient are reduced. The envelope of the waveform using MBS+HydroDyn shows a nearly constant damping. However, CFD predicts an excitation of the pitch motion at approximately 50 s < t < 100 s when the platform approaches the turning point of the surge oscillation. This phenomenon can be explained by the interaction of the platform with its own wake. Fig. 7 and 8 illustrate the flow field at different time steps and depths.

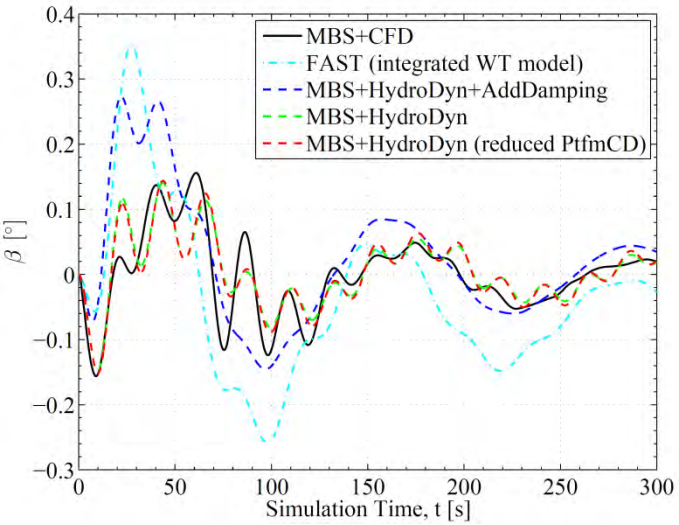

Fig. 6: Platform pitch motion

In general, the flow can be characterized by means of the Reynolds number given for a cylinder in Eq. 2. The maximum is *Re* (*D* = 9.4 m) = $9.8 \cdot 10^6$ and occurs at the maximum platform velocity in surge of approximately *v* (*t* = 27 s) = 0.9 m/s. Thus, turbulent flow separation is predominant at the beginning of the simulation. Laminar-turbulent transition gains importance as the velocity decreases with time.

$$Re = \frac{\rho_{water} \cdot v \cdot D}{\mu_{water}} \tag{2}$$

Separated flow and resulting vortices can be found at the platform as highlighted in black in Fig. 7 by the vorticity. The back flow regions are demonstrated by the tangential velocity vectors (red). At *t* = 57 s the platform surge reaches a turning point and the floating system reverses the direction of motion. As time progresses the platform interacts with its wake while the vortices move around the platform as can be seen in Fig. 7 from top to bottom.

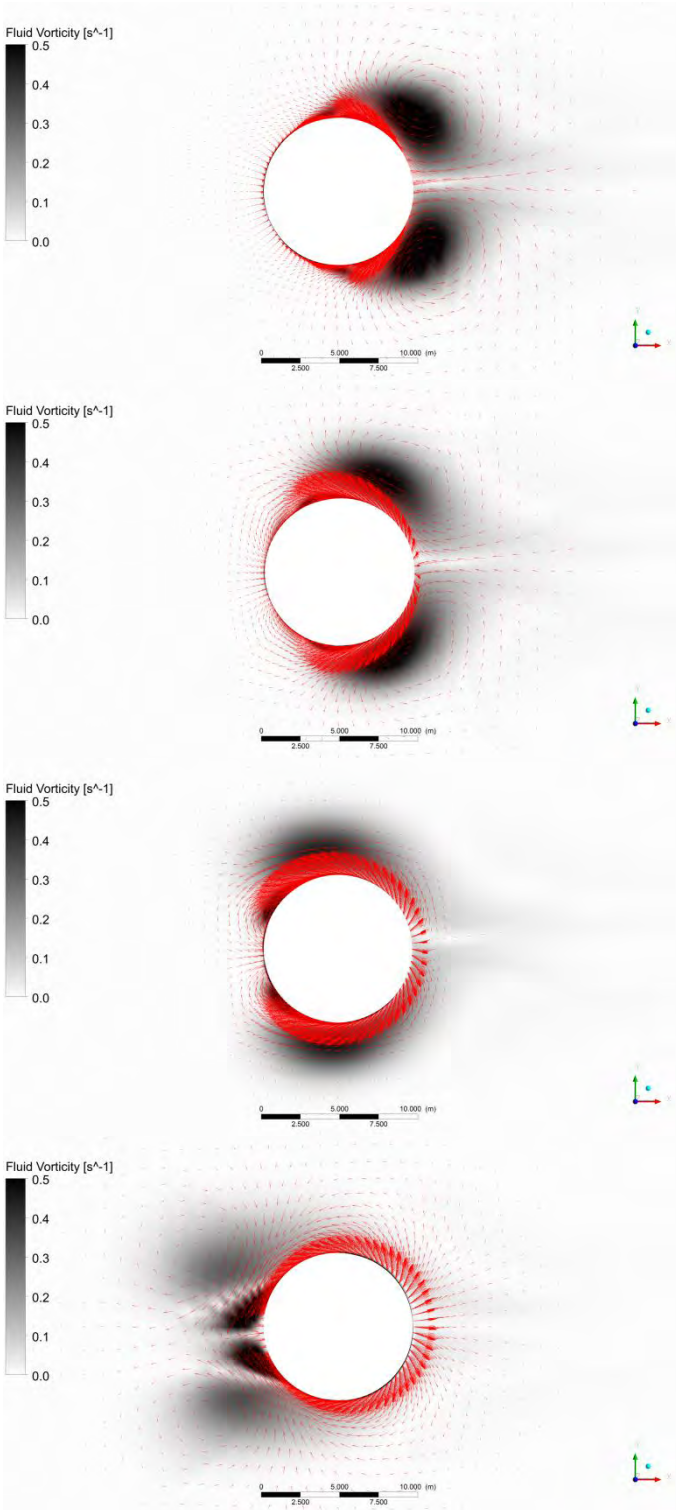

Fig. 7: Vorticity (black) and tangential velocity vector (red) at *z* = -82.5 m (from top to bottom: *t* = 57 | 62 | 67 | 75 s)

The vortices form a three-dimensional vortex tube along the *z*-axis. The characteristics of the flow around the cylinder become three-dimensional at the bottom of the platform. Thus, vortex-induced forces that are distributed non-uniformly below and above the center of mass act on the platform body. The overall center of mass is located at *z* = -82.5 m. The resulting moment excites the pitch motion. The vorticity

and the tangential velocity are illustrated for t = 57 s in Fig. 8 from top to bottom for depths of z = -60, -82.5 and -105 m. The vortices are located closer to the platform surface at z = -105 m compared to z = -60 m indicating a resulting moment.
HydroDyn accounts for flow separation by means of velocity-dependent damping from Morison's equation (nonlinear viscous drag). It is driven by parameters that are determined empirically and thus represent a potential cause for differences between methods. However, dynamic effects due to three-dimensional flow around the platform and fluid-structure-interactions cannot be captured with linear hydrodynamics but by CFD.

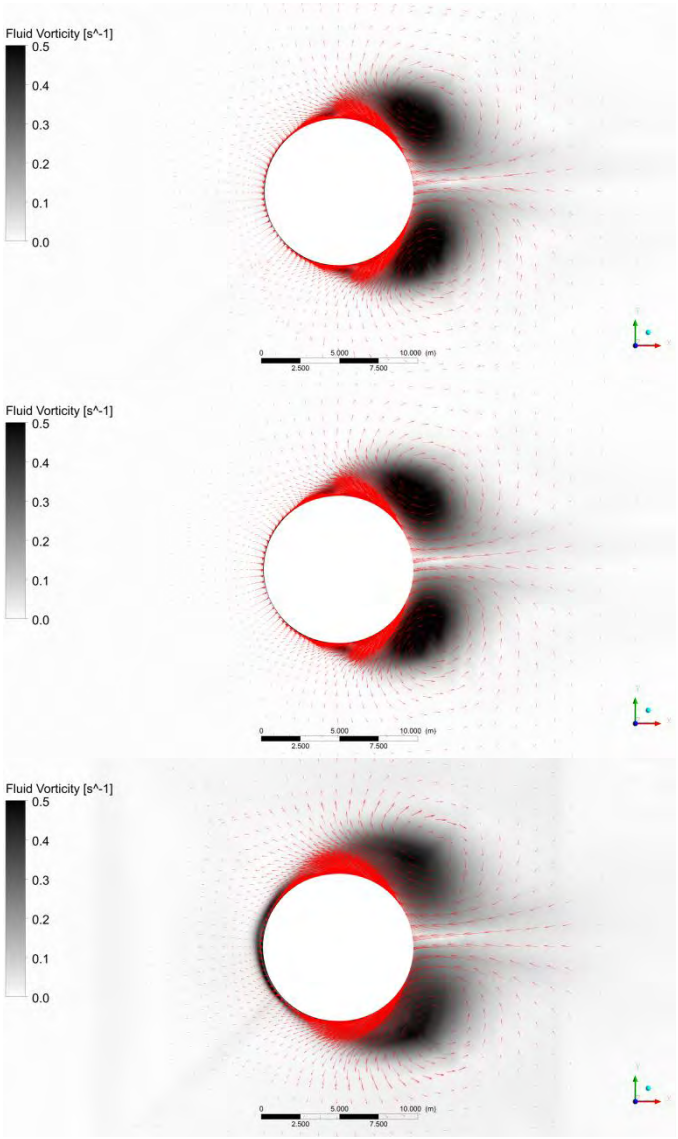

Fig. 8: Vorticity (black) and tangential velocity vector (red) at t = 57 s (from top to bottom: z = -60 | -82.5 | -105 m)

Pressure Distribution on the Hull

The loads on the hull of the platform are derived from the pressure distribution. In this load case no waves are present. Contributions from hydrostatics are most important and shown for the spar-buoy in Fig. 9.
The effect of the dynamic pressure at the stagnation point is negligible during the free-decay test due to the relatively small fluid velocity.

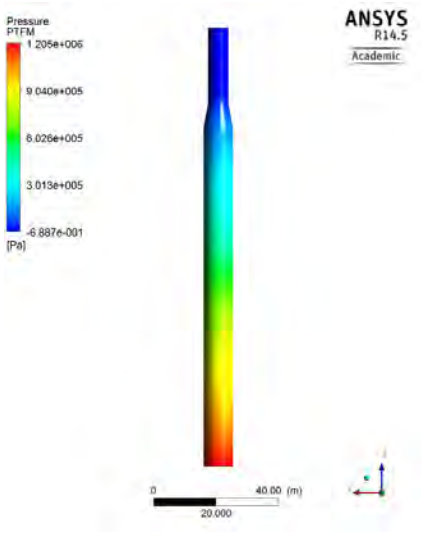

Fig. 9: Pressure distribution on the surface of the platform

OUTLOOK

Further simple load cases have to be performed for comparison between codes. The platform could be modeled as a rigid body in both CFD and MBS with a spring element connected to its center of mass to obtain restoring forces.
A fully integrated model of the OC3-Hywind system should be simulated to match the inertia and to take effects of aerodynamic damping into account.
The mutual influence of rigid body modes-of-motion of the floating system may be studied with additional simulations, for example, free-decay response in pitch.
More complex platform geometries need to be simulated like the OC4-DeepCwind semisubmersible (Robertson et al., 2012) consisting of several columns and pontoons. A modally reduced flexible FEM body of the platform may also be applied.
However, most important is the incorporation of incident waves via appropriate boundary conditions to analyze the effect of steep and breaking waves on the dynamics of FOWTs.

CONCLUSIONS

A method for the analysis of FOWT dynamics based on a coupling between CFD for flow-induced hydrodynamic loads and MBS is presented. A free-decay in surge of a conceptual FOWT is simulated. Results of the platform surge and pitch motion of MBS and CFD on the one hand and MBS and linear hydrodynamics on the other hand converge if the additional linear damping and the viscous drag coefficient are reduced. Pitch motion is small and differences in pitch-excitation are predicted by CFD due to vortex-induced forces on the platform. The pressure distribution on the surface of the platform is mainly driven by hydrostatics in this load case.

ACKNOWLEDGEMENTS

The coupling between CFX and SIMPACK used in this research has been developed by Stuttgart Chair of Wind Energy (SWE) in a project of Voith Hydro Ocean Current Technologies GmbH & Co. KG. The presented work was funded partially by the European Community's Seventh Framework Programme (FP7) under grant agreement number 295977 (FLOATGEN).

REFERENCES

Cordle, A, and Jonkman, J (2011). "State of the Art in Floating Wind Turbine Design Tools." *in 21st International Offshore and Polar Engineering Conference*. Maui, Hawaii, ISOPE, www.isope.org.

Ansys (2013). ANSYS 14.5 Theory Manual.

Arnold, M, Biskup, F, and Cheng, PW (2013). "Simulation of Fluid-Structure-Interaction on Tidal Current Turbines based on coupled Multibody and CFD Methods." *23rd International Offshore and Polar Engineering Conference*. Anchorage, Alaska, ISOPE, Vol 1..

HiPRWind (2013). "The HiPRWind Project." Retrieved February 1, 2013 (http://www.hyperwind.eu/).

Jonkman, B, and Jonkman, J (2010). "Documentation of Updates to FAST, A2AD and AeroDyn Released March 31, 2010, Including the Revised AeroDyn Interface." NREL, Golden, CO, USA.

Jonkman, J (2007). "Dynamics Modeling and Loads Analysis of an Offshore Floating Wind Turbine." Boulder, Colorado: Department of Aerospace Engineering Sciences, University of Colorado.

Jonkman, J (2010). "Definition of the Floating System for Phase IV of OC3." NREL, Golden, CO.

Jonkman, J, Butterfield, S, Musial, W, and Scott, G (2009). "Definition of a 5-MW Reference Wind Turbine for Offshore System Development." NREL, Golden, CO.

Jonkman, J, and Musial, W (2010). "Offshore Code Comparison Collaboration (OC3) for IEA Task 23 Offshore Wind Technology and Deployment Offshore Code Comparison Collaboration (OC3) for IEA Task 23 Offshore Wind Technology and Deployment." NREL, Golden, CO.

Matha, D, Schlipf, M, and Pereira, R (2011). "Challenges in Simulation of Aerodynamics , Hydrodynamics , and Mooring-Line Dynamics of Floating Offshore Wind Turbines." *in 21st Offshore and Polar Engineering Conference*. Maui, Hawaii, ISOPE, Vol 1,.

Musial, W, and Butterfield, S (2004). "Future for Offshore Wind Energy in the United States." *in Proceedings of the EnergyOcean 2004 Conference*. Palm Beach, FL.

Recharge (2013). EWEA 2013 Day Four.

Robertson, A, Jonkman, J, Masciolam, M, Song, H, Goupee, A, Coulling, A, and Luan, C (2012). "Definition of the Semisubmersible Floating System for Phase II of OC4." NREL, Golden, CO.

Schildhauer, M (2011). "Simulation von Fluid-Struktur-Interaktion mit ANSYS CFX." Hochschule für Technik, Wirtschaft und Kultur Leipzig.